Hybridization effects and bond-disproportionation in the bismuth perovskites

Kateryna Foyevtsova,[1,2] Arash Khazraie,[1,2] Ilya Elfimov,[1,2] and George A. Sawatzky[1,2]

[1]*Department of Physics & Astronomy, University of British Columbia, Vancouver, British Columbia V6T 1Z1, Canada*
[2]*Quantum Matter Institute, University of British Columbia, Vancouver, British Columbia V6T 1Z4, Canada*

(Dated: October 6, 2014)

We propose a microscopic description of the bond-disproportionated insulating state in the bismuth perovskites $X\mathrm{BiO_3}$ (X=Ba, Sr) that recognizes the bismuth-oxygen hybridization as a dominant energy scale. It is demonstrated using electronic structure methods that the breathing distortion is accompanied by spatial condensation of hole pairs into local, molecular-like orbitals of the A_{1g} symmetry composed of O-2p_σ and Bi-6s atomic orbitals of collapsed $\mathrm{BiO_6}$ octahedra. Primary importance of oxygen p-states is thus revealed, in contrast to a popular picture of a purely ionic $\mathrm{Bi^{3+}/Bi^{5+}}$ charge-disproportionation. Octahedra tilting is shown to enhance the breathing instability by means of a non-uniform band-narrowing. We argue that formation of localized states upon breathing distortion is, to a large extent, a property of the oxygen sublattice and expect similar hybridization effects in other perovskites involving formally high oxidation state cations.

PACS numbers: 74.20.Pq,74.70.-b,71.30.+h,71.45.Lr

arXiv:1410.0945v1 [cond-mat.mtrl-sci] 3 Oct 2014

The physics of perovskite compounds, featuring $B\mathrm{O_6}$ octahedra (B=cation) as building blocks, is exceptionally rich. The perovskites can be driven through a variety of structural, electronic, and magnetic phase transitions and are hosts to such intriguing states of matter as high-transition-temperature (T_c) superconductivity [cuprates[1], bismuth perovskites $X\mathrm{BiO_3}$ (X=Ba, Sr) [2–4]], a pseudo-gap state with strongly violated Fermi-liquid properties (cuprates[5]), and a spin/charge density wave [rare-earth nickelates $R\mathrm{NiO_3}$ (R=rare-earth atom) [6]], to name a few. It is appealing to relate the diverse physical properties observed across the perovskite family of materials with the individual characteristics of the cation B. The latter can be magnetic (Cu in the cuprates) or not (Bi in the bismuth perovskites), orbitally active (Mn in the manganites[7]) or not (Cu, Bi), prone to strong electronic correlations (transition-metal elements Cu and Ni) or not (Bi). With the due appreciation of the cation factor, there are, however, many striking similarities among different perovskite families suggesting an equally important role of their common structural framework. A vivid example is the transition into a bond-disproportionated insulating phase found in both the bismuthates and the rare-earth nickelates, in which oxygen plays an extremely important role[8–11]. Observations of this kind have given rise to theories aimed at a unified description of the perovskites, where the various competing phases emerge from polaronic and bipolaronic excitations of the polarizable oxygen sublattice.

While it is a common practice within this approach to assume that the only effect of electron-phonon coupling is variation of on-site energies, in this Letter we demonstrate that the effects due to hybridization between the oxygen-p orbitals and cation orbitals can be even more important. For this purpose, we focus on the bismuth perovskites $X\mathrm{BiO_3}$ where the analysis is greatly facilitated by the fact that the Bi ion valence states are non-magnetic, relatively weakly correlated, orbitally non-degenerate, and, to a first approximation, not affected by spin-orbit coupling (the Bi-6p states are above the Fermi level). Yet, we believe that our findings have broader implications for the perovskites in general.

The bismuth perovskites $\mathrm{BaBiO_3}$ and $\mathrm{SrBiO_3}$ are transition-metal-free high-T_c superconductors (when doped with holes) with intimately interlinked electronic and structural phase transitions. At low temperature, the parent compounds are insulators with certain characteristic distortions from an ideal cubic perovskite crystal structure. Namely, the $\mathrm{BiO_6}$ octahedra collapse and expand alternately along all three cubic crystallographic directions resulting in *disproportionated Bi-O bond distances*, a so-called *breathing* distortion. Simultaneously, they rigidly rotate and tilt to accommodate the Sr or Ba ions. The insulating bond-disproportionated state is often interpreted in terms of a charge-density wave. It is speculated that the Bi ions, whose nominal valency is 4+, disproportionate into $\mathrm{Bi^{3+}}$ and $\mathrm{Bi^{5+}}$[12–16] to avoid having a single electron in the 6s shell. This picture, however, is not supported experimentally[17–19] and is not consistent with the strongly covalent nature of the Bi-O bonding on one hand and the on-site repulsion effects on the other[20, 21]. To stress the importance of these two factors (covalency and on-site repulsion), a useful analogy with the nickelates can be drawn. There, the $3d^7$ configuration of Ni with one electron in the e_g doublet is similarly disfavored. As was originally suggested by Mizokawa *et al.*[8] and later shown in Refs. 9–11, electronic correlations, strong nickel-oxygen hybridization, and a negative charge-transfer gap result in holes preferring to occupy oxygen sites rather than nickel sites. In a combination with electron-phonon coupling to a lattice distortion of the breathing type, this promotes a $(d^8\underline{\mathrm{L}}^2)_{S=0}(d^8)_{S=1}$ configuration instead of the classical charge-disproportionated $(d^6)_{S=0}(d^8)_{S=1}$

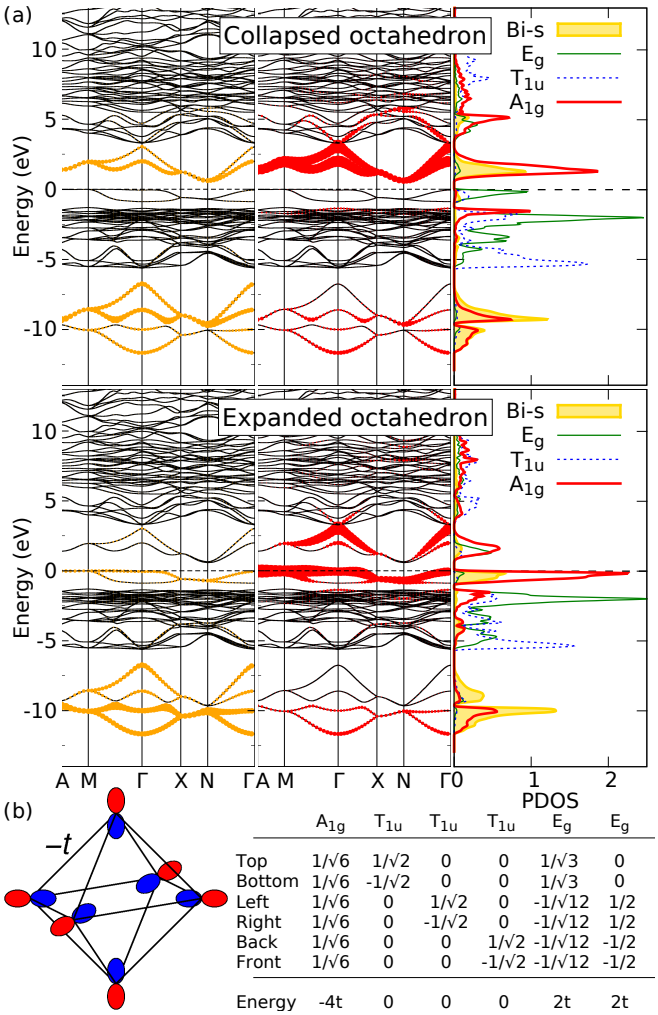

	A_{1g}	T_{1u}	T_{1u}	T_{1u}	E_g	E_g
Top	1/√6	1/√2	0	0	1/√3	0
Bottom	1/√6	-1/√2	0	0	1/√3	0
Left	1/√6	0	1/√2	0	-1/√12	1/2
Right	1/√6	0	-1/√2	0	-1/√12	1/2
Back	1/√6	0	0	1/√2	-1/√12	-1/2
Front	1/√6	0	0	-1/√2	-1/√12	-1/2
Energy	-4t	0	0	0	2t	2t

FIG. 1: (a) LDA electronic structure of $SrBiO_3$ projected onto the Bi-6s orbital and combinations of the O-p_σ orbitals of a collapsed (top) and expanded (bottom) BiO_6 octahedron. For the doublet E_g and the triplet T_{1u}, only one projection is shown. The Fermi level is set to zero, and PDOS stands for projected density of states and is given in states/eV/cell. (b) An octahedron of O-p_σ orbitals coupled via nearest-neighbor hopping integrals $-t$ and its eigenstates.

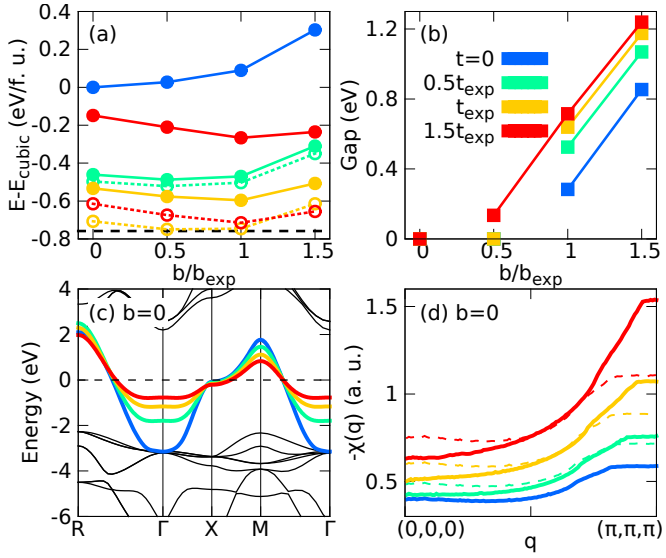

FIG. 2: (a), (b): LDA characterization of $SrBiO_3$ model structures with varying degrees of the BiO_6 octahedra's tilting, t, and breathing, b: (a) total energy per formula unit (f. u.) and (b) charge gap. In (a), solid lines and filled circles (dashed lines and open circles) represent model structures with fixed (relaxed) Sr atoms. The horizontal dashed line marks the energy of the experimental $SrBiO_3$ structure. (c), (d): The effect of tilting on (c) the half-filled band and on (d) the static susceptibility $\chi(\mathbf{q}, \omega = 0)$, at zero breathing. In (d), solid (dashed) lines represent calculations where nonlinear effects due to tilting are (are not) taken into account.

state (L=ligand hole, S=total on-site spin).

In the light of the above, here we investigate the nature of the insulating bond-disproportionated state in the bismuthates from the perspective of strong Bi-6s/O-2p hybridization using density functional theory (DFT) and local density approximation (LDA)[22]. We begin with highlighting basic features of the bismuthates' electronic structure [21, 23–32]. Since the LDA bandstructures of $BaBiO_3$ and $SrBiO_3$ are almost identical[22], in the following we will concentrate on $SrBiO_3$. The Bi-6s and O-2p orbitals strongly hybridize to create a broad band manifold near the Fermi level E_F extending from -14 to 3 eV [Fig. 1 (a)]. The upper band of this manifold is a mixture of the Bi-6s orbitals and the σ 2p orbitals of the oxygens, *i. e.*, the O-2p orbitals with lobes pointing towards the central Bi[33]. This upper band is half-filled as a result of *self-doping*: the 18 2p states of three oxygen ions and the two 6s states of a Bi ion are short of one electron to be fully occupied. Upon breathing, this band splits producing a charge gap. We note that even in the bond-disproportionated state, the bismuthates are very far from the ionic limit of pure Bi^{3+} and Bi^{5+}. The self-doped holes reside predominantly on the oxygen-p_σ orbitals, a situation similar to that in the nickelates. Below, we will infer the exact distribution of holes by analysing the DFT data in more detail.

In our further analysis, we will be guided by the following considerations. First, cation valence states of a given symmetry will be strongly hybridized with only certain combinations of surrounding O-p orbitals, the Zhang-Rice singlet in the cuprates being an example[34]. Thus, a spherically symmetric Bi-s orbital should couple only to the A_{1g} (*i. e.*, fully symmetric) combination of the p_σ orbitals of the surrounding oxygen atoms [Fig. 1 (b)]. Hoppings to any other combination of the O-p orbitals cancel out by symmetry. Second, since the Bi-6s orbitals are quite extended, the hybridization between the Bi-s and O-A_{1g} orbitals is very strong and even becomes a

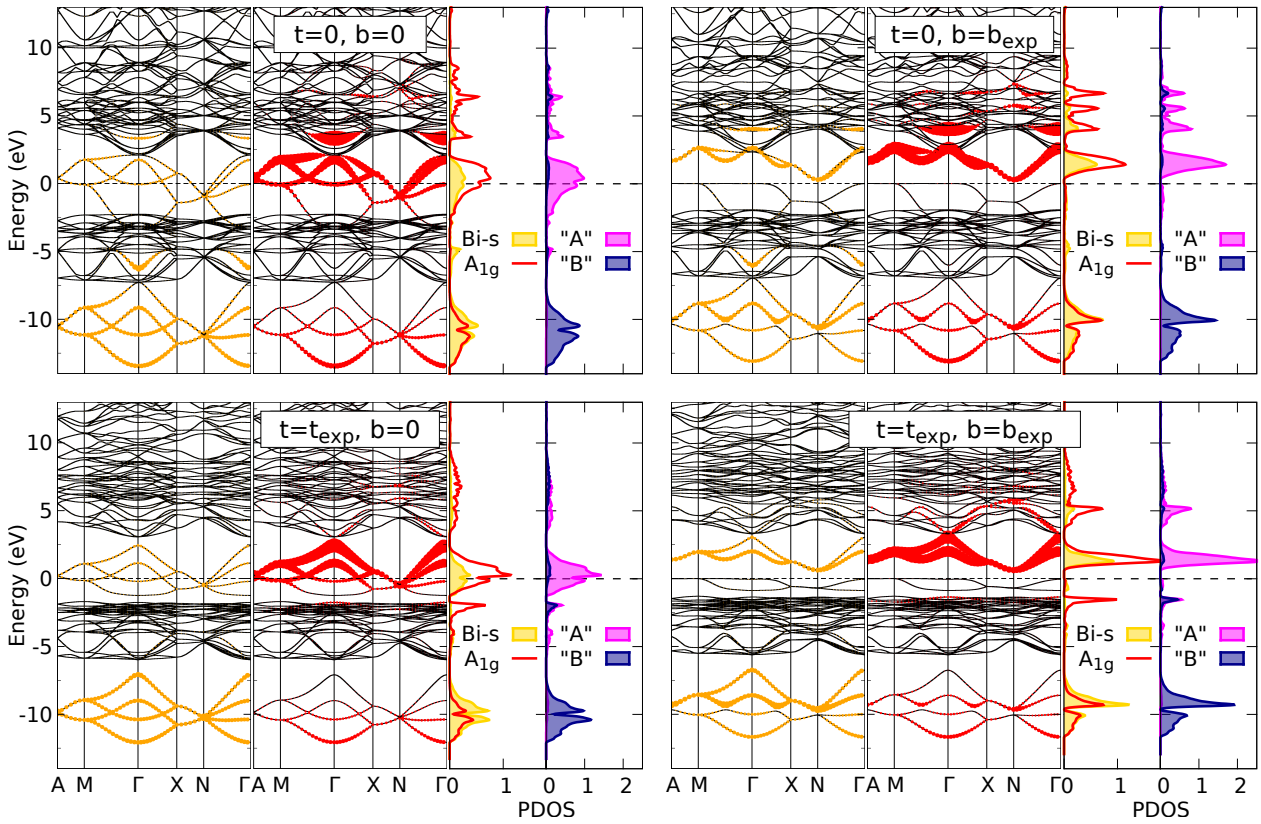

FIG. 3: LDA electronic structure of $SrBiO_3$ as a function of breathing b and tilting t. Projections are made onto the Bi-6s orbital and the A_{1g} combination of the O-p_σ orbitals of a collapsed BiO_6 octahedron, as well as their bonding ("B") and anti-bonding ("A") combinations.

dominant effect. Third, in the bond-modulated phase, hybridization within a collapsed (expanded) BiO_6 octahedron is strongly enhanced (suppressed), resulting in a formation of *local, molecular-like orbitals* on the collapsed octahedra.

We are able to observe all of these effects in our DFT results by projecting the LDA single-particle eigenstates onto the combinations of O-p_σ orbitals. Let us first focus of the *collapsed* octahedra. In the top panel of Figure 1 (a), one finds the Bi-6s and O-A_{1g} characters at $\sim$ 2 eV and at ~ -10 eV. The difference, $\sim$ 12 eV, is mainly a result of the hybridization splitting between the bonding and anti-bonding combinations, which indeed turns out to be the dominant energy scale for $SrBiO_3$. The anti-bonding combination is strongly peaked in the lowest two conductance bands throughout the whole Brillouin zone. In contrast, the location of the anti-bonding A_{1g} combinations of the *expanded* octahedra (bottom panel) is rather diffuse, with some weight seen both below and above E_F depending on the position in the Brillouin zone. This indicates that the metal-insulator transition with bond-disproportionation in the bismuthates should be understood as a pairwise spatial condensation of holes into the anti-bonding A_{1g} molecular orbitals of the collapsed octahedra. The small charge-disproportionation between the Bi ions (± 0.15 e inside the Bi muffin tin spheres) appears to be a *marginal side effect* of such hole condensation. Such a state, which resembles the $(d^8\underline{L}^2)_{S=0}$ singlet proposed for the nickelates, was also hypothesized in Ref. 35.

It is interesting to trace the evolution of the LDA projected density of states as a function of breathing b and tilting t. For this, we prepare a set of $SrBiO_3$ model structures with varying degrees of b and t[22]. In Figures 2 (a) and (b), the model structures are characterized in terms of, respectively, the total energy and the charge gap calculated within LDA. Parameters b and t are given with respect to the experimentally observed distortions $b_{\rm exp}$ and $t_{\rm exp}$. We find that a finite t is required to stabilize the breathing distortion. Although this result is known to be sensitive to details of DFT calculations[26], the absence of the breathing instability at zero tilting can be qualitatively understood in terms of a missing linear component in the elastic energy of an oxygen atom positioned between two Bi atoms. With increasing t, the equilibrium b shifts to higher values [Fig. 2 (a)], while the charge gap opens sooner as a function of b [Fig. 2 (b)]. We conclude, in agreement with

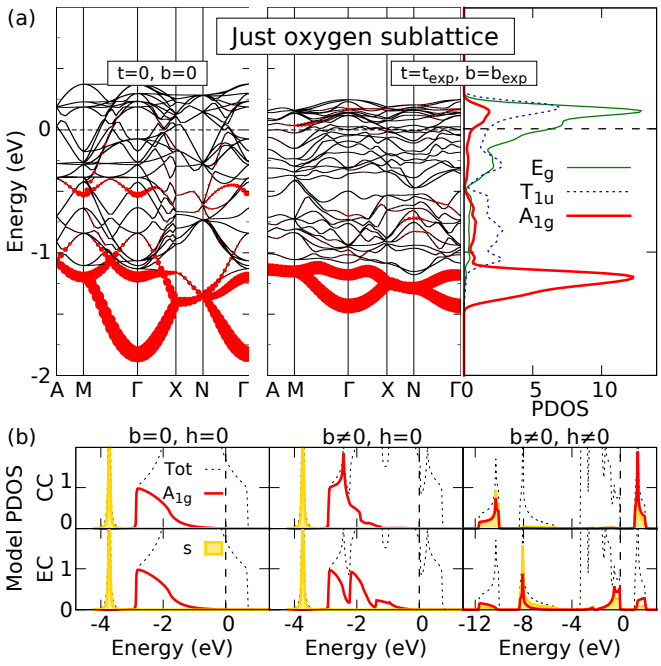

FIG. 4: (a) LDA electronic structure of the oxygen sublattice of $SrBiO_3$. Projections are made onto combinations of the O-p_σ orbitals of a collapsed O_6 octahedron. (b) Model density of states as a function of breathing b and hybridization between s- and p-orbitals h. CC (EC) stands for a collapsed (expanded) p-site cage. The model states are 90% filled, *i. e.*, there is one hole per s-orbital; Fermi energy is set to zero and marked with black dashed vertical lines.

previous DFT studies[25, 26, 30], that tilting enhances the breathing instability, through a mechanism yet to be discussed. Interestingly, letting Sr atoms relax from the high-symmetry positions (while keeping b and t fixed) can significantly lower the total energy for structures with high t [open circles in Fig. 2 (a)]. For the $(b_{\rm exp}, t_{\rm exp})$ structure, for instance, the energy drop is 0.15 eV per formula unit.

Figure 3 presents projections onto collapsed octahedra for the $(0,0)$, $(b_{\rm exp},0)$, $(0,t_{\rm exp})$, and $(b_{\rm exp},t_{\rm exp})$ structures. Here, the bonding ("B") and anti-bonding ("A") combinations of the Bi-6s and O-A_{1g} orbitals are shown explicitly. An important observation is that even with no breathing a major portion of the anti-bonding orbital weight is above E_F. Thus, the system is *predisposed* to hole condensation. The breathing distortion just makes collapsed octahedra more preferable for the holes to go to. On the other hand, the primary role of the tilting distortion is to reduce the bandwidth. This band-narrowing, however, is very *non-uniform* leading to certain important consequences, as will be discussed later.

Formation of well-defined molecular O-A_{1g} states on collapsed octahedra is a property of the oxygen sublattice. This is illustrated in Fig. 4 (a) which shows LDA calculations for an artificial system consisting of only the oxygen sublattice of $SrBiO_3$. Here, however, the A_{1g} states are the lowest in energy and fully occupied. It is the strong hybridization with the nearly degenerate Bi-6s states that pushes them above E_F. Upon hybridization, the 2 eV broad oxygen band and the essentially flat Bi-6s band will acquire a bandwidth of ~ 15 eV. As a further illustration, we can consider a simple tight-binding (TB) model for a two-dimensional perovskite-like lattice of $p_{\sigma,\pi}$-orbital sites and s-orbital sites, with nearest-neighbor $s-p$ and $p-p$ hoppings as found in $SrBiO_3$: $|t_{sp\sigma}| \sim 2.3$, $|t_{pp\sigma}| \sim 0.3$, and $|t_{pp\pi}| \sim 0.1$ eV[22]. Switching on the breathing distortion helps to form molecular A_{1g} states associated with collapsed p_σ-orbital cages at the bottom of the p-band [compare the left and central panels of Fig. 4 (b)]. Subsequent hybridization with the flat s orbitals, located right below the A_{1g} states, has a much stronger effect (since $|t_{sp}| \gg |t_{pp}|$) and pushes the anti-bonding $s-A_{1g}$ combination above E_F [right panel of Fig. 4 (b)].

Finally, we demonstrate the significance of the non-uniform nature of the tilting-induced band-narrowing. For this purpose, we calculate the static susceptibility $\chi(\mathbf{q},\omega=0)$ with the help of a single-band TB model for structures with zero breathing and varying tilting. Two kinds of TB models, describing the band crossing the Fermi level, are considered: (1) realistic $t \neq 0$ models closely following the LDA bands[22] and (2) $t \neq 0$ models uniformly rescaled with respect to the $t=0$ case such as to match the LDA bandwidth. In Fig. 2 (c), the band dispersions of the realistic models are plotted in the Brillouin zone of a small cubic cell so that the non-uniform nature of the t-induced band-narrowing is particularly clear: the changes at R, for example, are much smaller than at Γ. Using the realistic models and considering all the energies spanned by the band, we find a dominating susceptibility peak at $\mathbf{q}=(\pi,\pi,\pi)$ signaling breathing instability that quickly grows with increasing tilting [Fig. 2 (d), solid lines]. This growth is much quicker than it would be in the case of a uniform band-narrowing (compare with the dashed lines). This indicates that non-linear effects due to tilting, such as, possibly, approaching perfect nesting conditions, are very important for stabilizing the breathing distortion.

In summary, we have studied hybridization effects in the bismuth perovskites and their interplay with structural distortions such as breathing and tilting. It is shown that strong hybridization between the Bi-6s and O-2p orbitals precludes purely ionic charge disproportionation of a Bi^{3+}/Bi^{5+} form. Instead, the (self-doped) holes spatially condense into molecular-orbital-like A_{1g} combinations of the Bi-6s and O-2p_σ orbitals of *collapsed* BiO_6 octahedra, with predominantly O-2p_σ molecular orbital character. The tilting distortion is found to strongly enhance the breathing instability through (at least in part) an electronic mechanism, as manifested by a $\mathbf{q}=(\pi,\pi,\pi)$

peak in the static susceptibility $\chi(\mathbf{q}, \omega = 0)$.

It is expected that similar processes take place in other perovskites as well and can involve localized molecular orbitals of symmetries other than A_{1g}. Thus, in the rare-earth nickelates, the orbitals of relevance would be the E_g combinations of the O-p_σ orbitals hybridized with the Ni-e_g orbitals. Our model calculations indicate that two-dimensional systems, such as cuprates, can also exhibit hybridization effects of this kind.

[1] J. G. Bednorz and K. A. Müller, Zeitschrift fur Physik B Condensed Matter **64**, 189 (1986).

[2] R. J. Cava, B. Batlogg, J. J. Krajewski, R. Farrow, L. W. R. Jr., A. E. White, K. Short, W. F. Peck, and T. Kometani, Nature (London) **332**, 814 (1988).

[3] A. Sleight, J. Gillson, and P. Bierstedt, Solid State Communications **17**, 27 (1975), ISSN 0038-1098, URL http://www.sciencedirect.com/science/article/pii/0038109875903270.

[4] S. M. Kazakov, C. Chaillout, P. Bordet, J. J. Capponi, M. Nunez-Regueiro, A. Rysak, J. L. Tholence, P. G. Radaelli, S. N. Putilin, and E. V. Antipov, Nature **390**, 148 (1997).

[5] T. Timusk and B. Statt, Reports on Progress in Physics **62**, 61 (1999), URL http://stacks.iop.org/0034-4885/62/i=1/a=002.

[6] M. L. Medarde, Journal of Physics: Condensed Matter **9**, 1679 (1997), URL http://stacks.iop.org/0953-8984/9/i=8/a=003.

[7] Y. Tokura and N. Nagaosa, Science **288**, 462 (2000).

[8] T. Mizokawa, D. I. Khomskii, and G. A. Sawatzky, Phys. Rev. B **61**, 11263 (2000), URL http://link.aps.org/doi/10.1103/PhysRevB.61.11263.

[9] H. Park, A. J. Millis, and C. A. Marianetti, Phys. Rev. Lett. **109**, 156402 (2012), URL http://link.aps.org/doi/10.1103/PhysRevLett.109.156402.

[10] B. Lau and A. J. Millis, Phys. Rev. Lett. **110**, 126404 (2013), URL http://link.aps.org/doi/10.1103/PhysRevLett.110.126404.

[11] S. Johnston, A. Mukherjee, I. Elfimov, M. Berciu, and G. A. Sawatzky, Phys. Rev. Lett. **112**, 106404 (2014), URL http://link.aps.org/doi/10.1103/PhysRevLett.112.106404.

[12] T. M. Rice and L. Sneddon, Phys. Rev. Lett. **47**, 689 (1981), URL http://link.aps.org/doi/10.1103/PhysRevLett.47.689.

[13] D. Cox and A. Sleight, Solid State Communications **19**, 969 (1976), ISSN 0038-1098, URL http://www.sciencedirect.com/science/article/pii/0038109876906323.

[14] D. E. Cox and A. W. Sleight, Acta Crystallographica Section B **35**, 1 (1979), URL http://dx.doi.org/10.1107/S0567740879002417.

[15] C. M. Varma, Phys. Rev. Lett. **61**, 2713 (1988), URL http://link.aps.org/doi/10.1103/PhysRevLett.61.2713.

[16] I. Hase and T. Yanagisawa, Phys. Rev. B **76**, 174103 (2007), URL http://link.aps.org/doi/10.1103/PhysRevB.76.174103.

[17] J. de Hair and G. Blasse, Solid State Communications **12**, 727 (1973), ISSN 0038-1098, URL http://www.sciencedirect.com/science/article/pii/0038109873903232.

[18] A. F. Orchard and G. Thornton, J. Chem. Soc. Dalton Trans. p. 1238 (1977).

[19] G. K. Wertheim, J. P. Remeika, and D. N. E. Buchanan, Phys. Rev. B **26**, 2120 (1982), URL http://link.aps.org/doi/10.1103/PhysRevB.26.2120.

[20] W. A. Harrison, Phys. Rev. B **74**, 245128 (2006), URL http://link.aps.org/doi/10.1103/PhysRevB.74.245128.

[21] L. F. Mattheiss and D. R. Hamann, Phys. Rev. B **28**, 4227 (1983), URL http://link.aps.org/doi/10.1103/PhysRevB.28.4227.

[22] See Supplemental Material at [URL will be inserted by publisher] for technical details.

[23] M. Shirai, N. Suzuki, and K. Motizuki, Journal of Physics: Condensed Matter **2**, 3553 (1990), URL http://stacks.iop.org/0953-8984/2/i=15/a=012.

[24] N. Hamada, S. Massidda, A. J. Freeman, and J. Redinger, Phys. Rev. B **40**, 4442 (1989), URL http://link.aps.org/doi/10.1103/PhysRevB.40.4442.

[25] A. I. Liechtenstein, I. I. Mazin, C. O. Rodriguez, O. Jepsen, O. K. Andersen, and M. Methfessel, Phys. Rev. B **44**, 5388 (1991), URL http://link.aps.org/doi/10.1103/PhysRevB.44.5388.

[26] K. Kunc, R. Zeyher, A. Liechtenstein, M. Methfessel, and O. Andersen, Solid State Communications **80**, 325 (1991), ISSN 0038-1098, URL http://www.sciencedirect.com/science/article/pii/003810989190139M.

[27] K. Kunc and R. Zeyher, Phys. Rev. B **49**, 12216 (1994), URL http://link.aps.org/doi/10.1103/PhysRevB.49.12216.

[28] V. Meregalli and S. Y. Savrasov, Phys. Rev. B **57**, 14453 (1998), URL http://link.aps.org/doi/10.1103/PhysRevB.57.14453.

[29] R. Nourafkan, F. Marsiglio, and G. Kotliar, Phys. Rev. Lett. **109**, 017001 (2012), URL http://link.aps.org/doi/10.1103/PhysRevLett.109.017001.

[30] D. Korotin, V. Kukolev, A. V. Kozhevnikov, D. Novoselov, and V. I. Anisimov, Journal of Physics: Condensed Matter **24**, 415603 (2012), URL http://stacks.iop.org/0953-8984/24/i=41/a=415603.

[31] Z. P. Yin, A. Kutepov, and G. Kotliar, Phys. Rev. X **3**, 021011 (2013), URL http://link.aps.org/doi/10.1103/PhysRevX.3.021011.

[32] D. Korotin, D. Novoselov, and V. I. Anisimov, arXiv:1308.3057 (2013).

[33] In Fig. 1 (a), it appears as a set of four bands from -1 to 3 eV because of using a monoclinic $\sqrt{2}a \times \sqrt{2}a \times 2a$ (a=cubic lattice constant) supercell of $SrBiO_3$ with four formula units.

[34] F. C. Zhang and T. M. Rice, Phys. Rev. B **37**, 3759 (1988), URL http://link.aps.org/doi/10.1103/PhysRevB.37.3759.

[35] A. P. Menushenkov, K. V. Klementev, A. V. Kuznetsov, and M. Y. Kagan, Journal of Experimental and Theoretical Physics **93**, 615 (2001).